Point spread function fractions related to the ISOPHOT C100 and C200 arrays

R. J. Laureijs
ISO Data Centre, Astrophysics Division, ESA, Villafranca, Spain

Version 1.0
29 June 1999

Abstract

The fraction of the point spread function falling on a C100 or C200 pixel ($f_{psf}(d)$) has been determined per filter for a number of typical pointing configurations. For the C200 array these configurations are (1) at a distance of $92''$ pependicular to a side of a C200 pixel ($f_{psf}(92)$), (2) at a distance of $92\times\sqrt{2}''$ along the diagonal line ($f_{psf}(92\sqrt{2})$), and (3) when a point source is centred on the C200 array ($f_{psf}(array)$). For the C100 array the configurations are (1) at a distance of $46''$ perpendicular to a side of a C100 pixel ($f^1_{psf}(46)$), (2) at a distance of $46\times\sqrt{2}''$ along the diagonal line ($f^1_{psf}(46\sqrt{2})$), and (3) at a distance of $92''$ perpendicular to a side of a C100 pixel ($f^1_{psf}(92)$), The fractions were derived from calibration observations of asteroids, outer planets (Uranus and Neptune), and bright stars such as α Boo (HR5340). Comparison between the measured values and model computations show significant discrepancies for some of the C200 filters. The values of $f_{psf}(d)$ given in this report can be used to improve the point source photometry in minimaps and in source-background pointings, and to decide whether a source is extended. Examples of applications are presented.

1 Introduction

The absolute flux calibration of the ISOPHOT C-arrays has been obtained by comparing the FCS signal for a given FCS heating power with the signal of a calibration point source centred on a single pixel of a C-array. Depending on the filter used, it is assumed that a fixed fraction of the power of the calibration source is falling on a pixel. The value of this fraction was computed from a simple model for the point spread function of the ISO telescope. In the remainder of this report we refer to this fraction as $f_{psf}(0)$, we add the superscripts '1' or '2' to distinguish between the C100 and the C200 arrays, respectively. The values used for the ISOPHOT flux calibration are listed in Table 1. One should note that the "true" value of $f_{psf}(0)$ can be quite different from the ones listed in Table 1. However, for the correct point source calibration it is required that the values in Table 1 are used in observations that are similar to the calibration observations. I.e. for an unknown point source, the flux in a given filter should be obtained by centring the source on a pixel like in the calibration observations. Then the calibrated flux per pixel (in Jy/beam) should be divided by the corresponding $f_{psf}(0)$ to obtain the point source flux.

In other configurations, e.g. when centring the point source on the C200 array centre, an additional relationship is necessary between $f_{psf}(0)$ and the $f_{psf}(d)$ where d indicates the position of the point source w.r.t. the centre of a C200 pixel.

filter ID	wavelength μm	$f^1_{psf}(0)$	filter ID	wavelength μm	$f^2_{psf}(0)$
C_50	65	0.68	C_120	120	0.69
C_60	60	0.69	C_135	150	0.66
C_70	80	0.66	C_160	170	0.64
C_90	90	0.61	C_180	180	0.62
C_100	100	0.57	C_200	200	0.59
C_105	105	0.55			

Table 1: The assumed point spread function fractions for a point source centred on an ISOPHOT camera pixel ($f_{psf}(0)$). It is assumed that for a given filterband all pixels have the same $f_{psf}(0)$

In this report we determine the values for $f_{psf}(d)$ for a number of typical positions of a C200 pixel with respect to a point source. Fig. 1 illustrates the definitions of the different $f_{psf}(d)$.

There are several applications for $f_{psf}(d)$:

- To determine the source and background flux of point sources in C200 minimaps. Knowing the values of $f_{psf}(92)$ and $f_{psf}(92\sqrt{2})$ one can fit the flux distribution over the entire minimap. For example, assuming a point source positioned in the centre of a minimap then the flux of the source can be computed from:

$$F_\nu(src) = \frac{F^*_\nu(0') - F^*_\nu(92)}{(f^2_{psf}(0) - f^2_{psf}(92))}, \tag{1}$$

  and with background flux:

$$F^*_\nu(bck) = \frac{f^2_{psf}(0)F^*_\nu(92) - f^2_{psf}(92)F^*_\nu(0)}{(f^2_{psf}(0) - f^2_{psf}(92))}. \tag{2}$$

  Where the superscript(*) indicate the flux per pixel in Jy/beam, and $F^*_\nu(d)$ the (mean) flux at distance d in Jy/beam. It is implicitly assumed that the pointing accuracy is better than a few arcseconds so that flux variations due to pointing errors are negligible. The method can be more accurate than the "conventional" method where the background flux level is determined from positions far away from the source. This is because the uncertainty due to cirrus confusion and background inhomogeneities increases at larger distances from the source.

- To determine the point source flux when the source is centred on the C200 array. The source flux is given by the sum of the individual fluxes of the C200 pixels:

$$F_\nu(src) = \Sigma F^*_\nu(pix\ i)/f_{psf}(array) \tag{3}$$

  It is shown below that $f_{psf}(array)$ is hard to predict from present model calculations, so that an empirical value for each filter band is required.

- To decide whether a source is extended from maps that are not oversampled. In this report we present observed values of the pixel footprint at certain

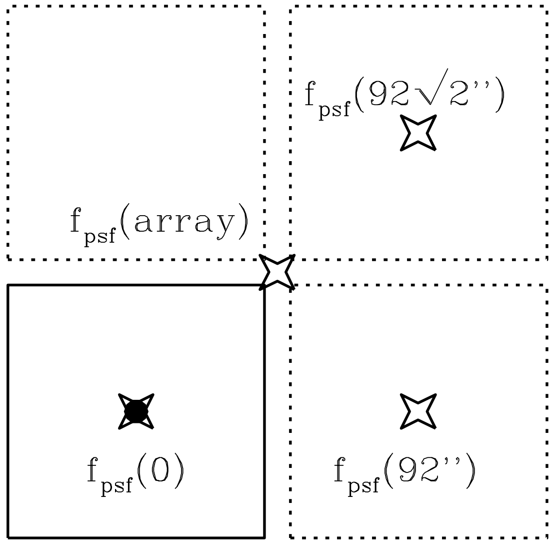

Figure 1: Schematic diagram to illustrate the definitions of the different $f_{psf}(d)$. The open square indicates a C200 pixel, the stars indicate the possible positions of a point source with respect to the pixel.

distances from the pixel centre with a high accuracy. Present deconvolution methods use a model footprint which - as we will see below - can deviate significantly at those positions for a given filterband.

2 Data processing and results

2.1 Signal processing

The data were processed using standard PIA V7.3.3 routines up to signal per chopper plateau level (SCP). We have included an additional correction for signal nonlinearities to be as close as possible to the PHT OLP8.4 calibration. In appendix A we have listed the targets and the corresponding TDTs. The targets have been selected mainly on the basis of their source-background contrast during the observations. To minimize the uncertainties due to background subtraction it was required that the target signal should be at least as strong as the background signal. For the determination of the background zero level we have taken either dedicated background observations or pointings sufficiently far away from the centre in the minimaps themselves. The analysis showed that signals taken with different reset interval cannot be compared because the (systematic) uncertainties in the reset-interval correction are generally too large for the accuracies required in the determination of $f_{psf}(d)$. We therefore rejected data sets with measurements taken with different reset interval unless the source-background contrast is very high (> 10).

2.2 C200 analysis and results

Depending on the observing mode, some corrections were made for baseline variations that are linear in time. These variations are due to either a gradient in the background or due to a steady responsivity drift. Most data sets consist of a minimap (in most cases a 6×2 raster map in spacecraft coordinate frame with 92″ step in both raster directions) and a number of source and background pointings collected close in time. We have added several data sets of asteroids to obtain sufficient statistics for the determination of of $f_{psf}(92)$ and $f_{psf}(92\sqrt{2})$.

In all cases we have obtained the ratios:

$$f^2_{psf,i}(d)/f^2_{psf,i}(0) \;=\; s_i(d)/s_i(0) \qquad (4)$$

where i stands for a given C200 pixel and $s_i(d)$ the signal (in V/s) at distance d from the calibration point source. By normalizing each pixel to its peak signal, flat field uncertainties have been avoided. Both $s_i(d)$ and $s_i(0)$ should be measured close in time. The final ratio per filter observation is obtained from either the average or summation of the four pixels:

$$f^2_{psf}(d)/f^2_{psf}(0) \;=\; \frac{\Sigma(s_i(d)/s_i(0))}{4} \qquad for\ d = 92'',\, 92\sqrt{2}'', \qquad (5)$$

and,

$$f^2_{psf}(array)/f^2_{psf}(0) \;=\; \Sigma(s_i(d)/s_i(0)) \qquad for\ d = 46\sqrt{2}'' \qquad (6)$$

The uncertainty of a determination was estimated from the consistency among the pixels:

- for $f^2_{psf}(92)$ and $f^2_{psf}(92\sqrt{2})$ the uncertainty for each determination is the rms of the 4 pixel values.
- for $f^2_{psf}(array)$ the uncertainty is 2 times the rms of the 4 pixel values.

In both cases it is assumed the beamprofile is point symmetric. Consequently the 4 values of $f_{psf}(d)/f_{psf}(0)$ should be identical and that pixel to pixel variations are purely statistical. In the following section we discuss the validity of this assumption. The final values are the weighted averages of the individual measurements, the uncertainty is the weighted rms of the distribution, thus not divided by $\sqrt{N}$. The results are given in Tables 2 and 3.

filter ID	wavelength (μm)	$f_{psf}(92)/f_{psf}(0)$ **this study**	$f_{psf}(92)/f_{psf}(0)$ **model**
C_120	120	0.0589±0.0033	0.0645
C_135	150	0.0763±0.0024	0.0643
C_160	170	0.0656±0.0032	0.0679
C_180	180	0.0946±0.0042	0.0689
C_200	200	0.0989±0.0044	0.0789

Table 2: The point spread function fractions for $d = 92$ ($f_{psf}(92)$).

2.3 C100 analysis and results

The same type of analysis as for C200 has been performed for the C100 array. We also wanted to investigate whether the $f^1_{psf}(array)$ for C100 used in OLP7 and earlier are valid. We have determined $f^1_{psf}(46)$ and $f^1_{psf}(46\sqrt{2})$ which are equivalent to the C200 $f^2_{psf}(92)$ and $f^2_{psf}(92\sqrt{2})$. In addition, we determined $f^1_{psf}(92)$ which is the fraction of the psf for a pixel positioned 92″ away from a point source perpendicular to a side of the pixel. For the observations we have used raster maps (3×5 points, 46″ step in both directions in spacecraft orientation) on HR5340, Pallas, and Vesta. The results are listed in Table 5.

filter ID	wavelength (μm)	$f_{psf}(92\sqrt{2})/f_{psf}(0)$ **this study**	$f_{psf}(92\sqrt{2})/f_{psf}(0)$ **model**
C_120	120	0.0161±0.0015	0.0169
C_135	150	0.0266±0.0023	0.0267
C_160	170	0.0298±0.0027	0.0328
C_180	180	0.0371±0.0020	0.0354
C_200	200	0.0525±0.0017	0.0420

Table 3: The point spread function fractions for $d = 92\sqrt{2}$ ($f_{psf}(92\sqrt{2})$).

filter ID	wavelength μm	$f_{psf}(array)$ **this study**	$f_{psf}(array)$ **model**	$f_{psf}(array)$ **OLP7 value**
C_120	120	0.498±0.028	0.814	0.574
C_135	150	0.568±0.029	0.846	0.668
C_160	170	0.528±0.021	0.733	0.708
C_180	180	0.612±0.046	0.818	0.972
C_200	200	0.693±0.020	0.655	1.054

Table 4: The point spread function fractions for the C200 array centre ($f_{psf}(array)$).

3 Comparison with model predictions

3.1 Model description

The model predictions by U. Herbstmeier ([1], [2]) comprised the computation of the ISO point spread function (psf) based on the ISO primary mirror, secondary mirror, and tripod. The detector footprint was derived by a subsequent convolution of the psf with the geometrical areas of the detector pixels. In the calculations the actual filter transmission curves as measured in laboratory were used to account for the spectral width of the bands. A flat energy distribution for the source was assumed.

3.2 C200 data

The model values are included in Tables 2, 3, and 4 and were taken from the Cal G footprint files. The computed and measured values of $f_{psf}(d)$ are plotted in Figs. 2 and 3.

The model values of $f_{psf}(92\sqrt{2})$ at 120, 150 and 170 μm match very well the measurements within the observational uncertainties. At 180 and 200 μm, the measured $f_{psf}(92\sqrt{2})$ is larger ($\leq$ 20%) than predicted suggesting a slightly wider footprint distribution at the longest wavelengths. For $f_{psf}(92)$ we find slightly lower measured values at 120 and 170 μm whereas at 150, 180, and 200 μm the measured values are significantly larger than predicted. The discrepancy is largest at 180 μm (28%).

In case of $f_{psf}(array)$ (Fig. 3) all measured values are lower than predicted except for C_200. This trend is contrary to the $f_{psf}(92)$ and $f_{psf}(92\sqrt{2})$ measurements which are either equal or higher than the predictions. The largest discrepancies are found at the shortest wavelengths (up to 64% at 120 μm). The relatively lower value at 170 μm is also apparent in the predictions, giving confidence in the measurements.

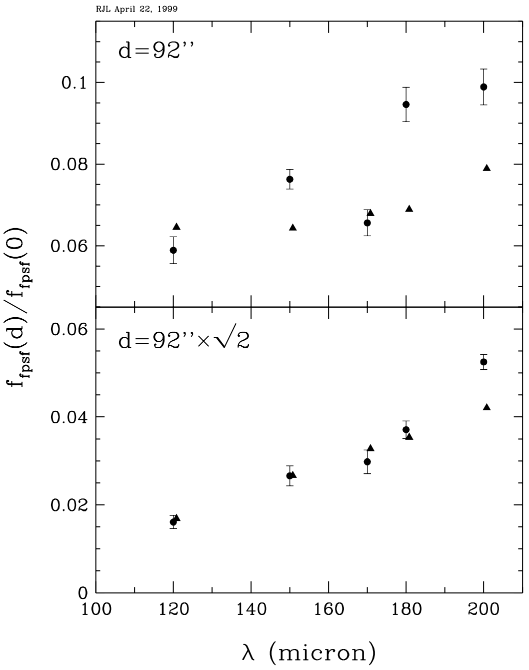

Figure 2: The values of $f_{psf}(92)$ (upper panel) and $f_{psf}(92\sqrt{2})$ (lower panel) as a function of central wavelength of each C200 filter, filled circles: this study, triangles: model calculation.

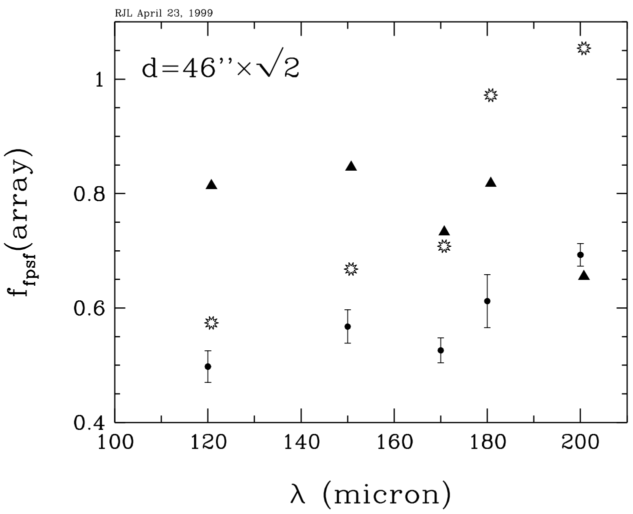

Figure 3: The values of $f_{psf}(array)$ as a function of central wavelength; filled circles: this study, stars: OLP7 values, triangles: model calculation.

filter ID	λ_c (μm)	$f^1_{psf}(46)/f^1_{psf}(0)$	$f^1_{psf}(46\sqrt{2})/f^1_{psf}(0)$	$f^1_{psf}(92)/f^1_{psf}(0)$
C_50	65	0.0465±0.0045	0.0077±0.0012	0.0019±0.0008
C_60	60	0.0375±0.0030	0.0057±0.0004	0.0015±0.0006
C_70	80	0.0632±0.0049	0.0171±0.0024	0.0025±0.0011
C_90	90	0.0553±0.0063	0.0187±0.0022	0.0014±0.0010
C_100	100	0.0598±0.0068	0.0292±0.0030	0.0020±0.0013
C_105	105	0.0699±0.0080	0.0336±0.0036	0.0037±0.0014

Table 5: The measured point spread function fractions for pixels in the C100 array.

3.3 C200 consistency checks

The fraction of the psf falling on each pixel when centring a point source on the array has been assessed from the following quantity:

$$f^{2,*}_{fpsf}(array, i) = f^2_{fpsf,i}(array)/\Sigma f^2_{fpsf,i}(array) \tag{7}$$

where the superscript (*) indicates the normalised value. In the ideal situation, the point source flux should be homogeneously distributed and $f^*_{fpsf}(array, i)$ should be 0.25 for all pixels. For each observation we have initially determined $f^*_{fpsf}(array, i)$, and subsequently taken the sample average per pixel. The final uncertainty is the uncertainty of the pixel average. The results are presented in Table 6.

wave-length (μm)	$f^*_{psf}(array, 1)$	$f^*_{psf}(array, 2)$	$f^*_{psf}(array, 3)$	$f^*_{psf}(array, 4)$
120	0.202±0.013	0.212±0.020	0.360±0.026	0.225±0.005
150	0.203±0.014	0.222±0.009	0.348±0.012	0.227±0.009
170	0.208±0.023	0.237±0.016	0.324±0.020	0.231±0.010
180	0.208±0.012	0.241±0.001	0.340±0.008	0.210±0.005
200	0.244±0.013	0.247±0.013	0.284±0.012	0.227±0.007

Table 6: Measured values of $f^*_{psf}(array, i)$, see text for definition.

It can be seen that the fraction of the psf falling on pixel 1 is too low for all filters except C_200, as opposed to pixel 3 where the fraction is 3-11% too high. There seems to be an asymmetry in the illumination of the array, since pixel 1 is mounted opposite to pixel 3 with respect to the array centre. This result shows also that the estimated uncertainties of $f_{psf}(array)$ will be always higher due to the inhomogeneous illumination. At the longest wavelength, the illumination becomes more homogeneous, probably due to the larger Airy disk of the psf.

Another interesting cross check is the fraction of the psf falling on a 3x3 (92″ step) minimap area. This fraction can be computed from:

$$f_{psf}(3{\times}3) = f_{psf}(0) + 4f_{psf}(92) + 4f_{psf}(92\sqrt{2}) \tag{8}$$

The actual values are listed in Table 7 and plotted together with the predicted values in Fig. 4. The measurements are all less than 1.0 which shows that there is still a fraction of the psf falling outside the region. The predicted values are for all wavelengths lower than the measured ones. The biggest discrepancy is 12%

filter ID	wavelength μm	$f_{psf}(3\times3)$
C_120	120	0.8969±0.0050
C_135	150	0.9316±0.0044
C_160	170	0.8842±0.0054
C_180	180	0.9468±0.0057
C_200	200	0.9474±0.0055

Table 7: The derived point spread function fractions for a minimap area of $276'' \times 276''$, or 3×3 minimap.

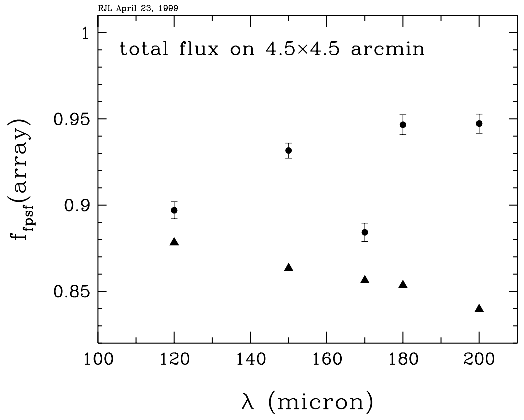

Figure 4: Total psf fractions on falling on a 3×3 minimap with $92''$ step in both directions, the filled circles are derived from the measurements but assuming the computed value of $f_{psf}(0)$ as given in Table 1, the triangles are obtained from the model by Herbstmeier.

at $200\,\mu$m. The best match between predicted and measured values of $f_{psf}(92)$ and $f_{psf}(92\sqrt{2})$ is found to be at 120 and 160 μm. The measured values at the other wavelengths are higher and can partly be explained by an overestimate of the background zero level. However, since we have measured the values of $f_{psf}(92)$ and $f_{psf}(92\sqrt{2})$ relative to $f_{psf}(0)$, we conclude that the value of $f_{psf}(0)$ as used in the absolute calibration (Table 7) - obtained from an different (earlier) footprint model - is probably higher than the actual value.

3.4 C100 data

For comparison we have obtained the $f^1_{psf}(d)$ values as computed by U. Herbstmeier [2], see Table 8. In Table 9 we list the total psf fraction falling on an area of 3×3 C100 pixels obtained by applying a similar summation as given in Eqn. 8. The configuration is identical to that of centring a point source on the C100 array, therefore we have included the values for $f^1_{psf}(array)$ as used in OLP.

Figs. 5 and 6 show a comparison between the measured and predicted values of the various $f^1_{psf}(d)$. It can be seen that the measured $f^1_{psf}(d)$ is in nearly all cases (except one) lower than the predictions. The measured $f^1_{psf}(92)$ is significantly smaller than the predictions, this can be due to a slight overestimate of the

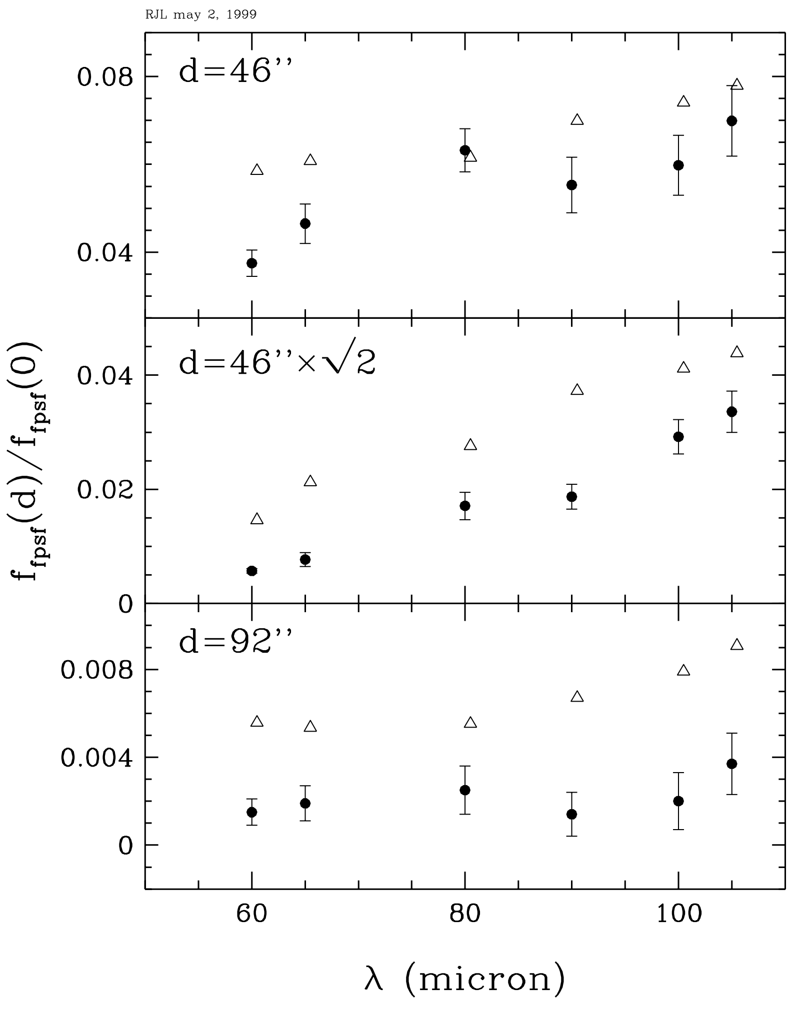

Figure 5: The values of $f^1_{psf}(46)/f^1_{psf}(0)$ (upper panel) $f_{psf}(46\sqrt{2})/f^1_{psf}(0)$ (middle panel), and $f_{psf}(92)/f^1_{psf}(0)$ as a function of central wavelength of each C100 filter, filled circles: this study, triangles: model calculation.

background. If this is the case one should be aware that the overestimate must be small, on average a fraction of a percent of the signal centred on the calibration source. This implies that the background uncertainty must be relatively smaller for the other values of $f^1_{psf}(d)$. Thus the discrepancies found for $f^1_{psf}(46)$, $f^1_{psf}(46\sqrt{2})$ and $f^1_{psf}(array)$ are most likely real.

filter ID	λ_c (μm)	$f^1_{psf}(0)$ **model**	$f^1_{psf}(46)$ **model**	$f^1_{psf}(46\sqrt{2})$ **model**	$f^1_{psf}(92)$ **model**
C_50	65	0.6354	0.0386	0.0135	0.0034
C_60	60	0.6633	0.0388	0.0097	0.0037
C_70	80	0.6157	0.0379	0.0170	0.0034
C_90	90	0.5664	0.0396	0.0211	0.0038
C_100	100	0.5441	0.0403	0.0224	0.0043
C_105	105	0.5287	0.0412	0.0232	0.0048

Table 8: The point spread function fractions as computed by U. Herbstmeier, ("model").

filter ID	λ_c (μm)	$f^1_{psf}(3\times3)$ **this work**	$f^1_{psf}(3\times3)$ **model**	$f^1_{psf}(3\times3)$ **OLP7**
C_50	65	0.828±0.006	0.844	0.912
C_60	60	0.809±0.004	0.857	0.918
C_70	80	0.872±0.007	0.835	0.902
C_90	90	0.790±0.008	0.809	0.900
C_100	100	0.773±0.008	0.795	0.892
C_105	105	0.778±0.010	0.786	0.884

Table 9: The point spread function fractions for an area of 3×3 C100 pixels, in the idealized case these f_{psf} values represent the psf fraction for a point source centred on the C100 array.

The values for $f^1_{psf}(array)$ as predicted by U. Herbstmeier are close (within 10%) of the measurements. However, the OLP7 values are always higher and at most 15% off the measured values. Therefore if our measured $f^1_{psf}(array)$ are correct, then OLP7 underestimates the C100 point source flux by at most 15%.

4 Examples

Example 1. In the dedicated serendipity calibration observations deep 4×4 (92″) step minimaps were performed on a number of galaxies. We have analyzed NGC6380 and NGC6140, the results are given in Table 10. For both targets the ratios $f_{psf}/f_{psf}(0)$ are in all cases significantly larger than the ones given in Tables 2 and 3. The optical images show that NGC6140 is more extended than NGC6381 and larger than 2′ diameter. The 170 μm minimaps confirm this observation.

References

[1] Herbstmeier U.: "C200 - Comparison between modelled and measured footprints - the derived parameters", ISOPHOT Internal Report 03 March 1998.

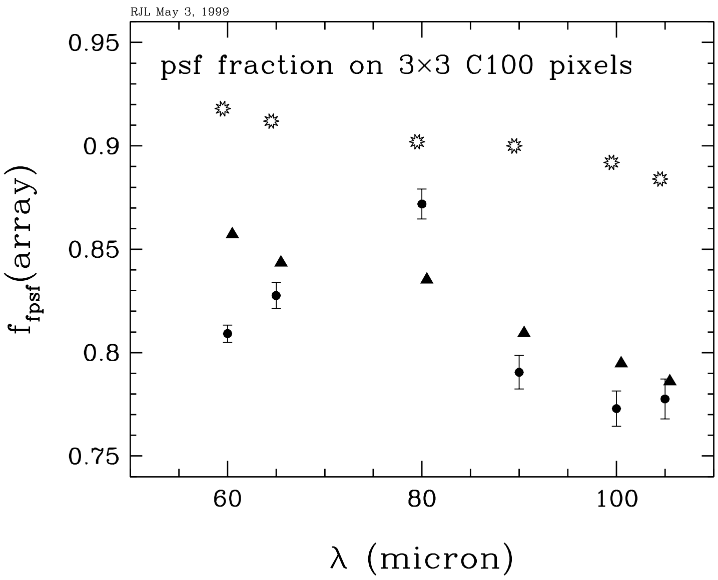

Figure 6: The fraction of the point source flux falling on 3×3 pixels aligned in the same way as in the C100 array. Filled circles: our measurements, triangles: from footprint model by U. Herbstmeier, stars: values used in OLP7 and earlier.

target	$f_{psf}/f_{psf}(0)$	pix 1	pix 2	pix 3	pix 4	mean	rms
NGC	$f_{psf}(92)/f_{psf}(0)$	0.435	0.322	0.351	0.311	0.355	0.048
6381	$f_{psf}(92\sqrt{2})/f_{psf}(0)$	0.176	0.095	0.154	0.124	0.137	0.031
NGC	$f_{psf}(92)/f_{psf}(0)$	0.232	0.116	0.174	0.147	0.167	0.042
6381	$f_{psf}(92\sqrt{2})/f_{psf}(0)$	0.057	0.019	0.062	0.031	0.042	0.018

Table 10: The point spread function fractions derived from minimaps of two galaxies taken at 170 μm (proposal: SERCAL02).

[2] Herbstmeier U.: "C100 - Comparison between modelled and measured footprints - the derived parameters", ISOPHOT Internal Report 03 March 1998.

A Input calibration observations for C200

target	TDT	wavelength	pix 1	pix 2	pix 3	pix 4	mean	rms
Ceres	07600000	120	0.087	0.100	0.197	0.115	0.497	0.086
Uranus	55204908	120	0.114	0.128	0.147	0.106	0.494	0.031
Ceres	57901808	120	0.106	0.093	0.204	0.122	0.526	0.086
Pallas	07300000	150	0.151	0.140	0.190	0.139	0.620	0.042
Ceres	07600000	150	0.082	0.107	0.167	0.113	0.468	0.062
Ceres	11101800	150	0.091	0.122	0.187	0.100	0.500	0.075
Ceres	59402708	150	0.131	0.118	0.217	0.151	0.617	0.077
Pallas	07300000	170	0.163	0.142	0.200	0.157	0.662	0.043
Ceres	07600000	170	0.068	0.102	0.161	0.113	0.444	0.066
Ceres	11101800	170	0.083	0.120	0.165	0.105	0.472	0.060
HR5340	45300701	170	0.088	0.179	0.208	0.106	0.581	0.100
Ceres	57902212	170	0.146	0.126	0.239	0.176	0.687	0.085
Hygiea	83201511	170	0.143	0.106	0.102	0.108	0.460	0.033
Ceres	07600000	180	0.107	0.134	0.197	0.122	0.560	0.068
Ceres	59402304	180	0.148	0.159	0.216	0.133	0.657	0.063
Herculina	03700000	200	0.139	0.191	0.182	0.141	0.653	0.047
Ceres	07600000	200	0.210	0.179	0.245	0.204	0.839	0.047
Ceres	11101800	200	0.138	0.167	0.210	0.140	0.656	0.058
Uranus	55204704	200	0.192	0.171	0.157	0.138	0.658	0.040
Ceres	57901304	200	0.169	0.145	0.196	0.162	0.673	0.037

Table 11: The target list and the individual measurements for the derivation of $f_{psf}(array)$.

target	TDT	wavelength	pix 1	pix 2	pix 3	pix 4	mean	rms
Ceres	09302314	120	0.018	0.011	0.007	0.008	0.011	0.004
HR5340	07707505	120	0.001	0.022	0.043	0.027	0.023	0.015
Neptune	13302502	120	0.010	0.008	0.019	0.012	0.012	0.004
Herculina	18203108	120	0.036	0.022	0.032	0.024	0.028	0.006
Vesta	24400908	120	0.016	0.014	0.022	0.012	0.016	0.004
Pallas	25101608	120	0.023	0.019	0.027	0.017	0.022	0.004
HR5340	27503008	120	0.030	0.010	0.025	0.034	0.025	0.009
Ceres	27505108	120	0.031	0.027	0.013	0.008	0.020	0.009
Uranus	32802805	120	0.014	0.008	0.017	0.010	0.012	0.003
Neptune	33502902	120	0.014	0.011	0.023	0.015	0.016	0.004
Uranus	55204908	120	0.016	0.014	0.017	0.012	0.015	0.002
Ceres	57901808	120	0.029	0.022	0.031	0.015	0.024	0.006
Ceres	09302011	150	0.034	0.025	-0.003	0.003	0.015	0.015
HR5340	07708111	150	-0.012	0.033	0.070	0.017	0.027	0.029
Ceres	111018	150	0.024	0.027	0.020	0.011	0.020	0.006
Neptune	15400602	150	0.019	0.017	0.031	0.021	0.022	0.005
Herculina	18203411	150	0.070	0.046	0.040	0.046	0.051	0.011
Vesta	24401211	150	0.032	0.020	0.033	0.020	0.027	0.006
Pallas	25101911	150	0.037	0.032	0.052	0.044	0.041	0.008
HR5340	27503311	150	0.045	0.006	0.007	0.063	0.030	0.024
Ceres	27505411	150	0.035	0.042	0.012	0.014	0.026	0.013
Uranus	32803411	150	0.024	0.018	0.028	0.021	0.023	0.004
Neptune	33503205	150	0.025	0.034	0.039	0.026	0.031	0.006
Ceres	59402708	150	0.032	0.020	0.048	0.028	0.032	0.010
Ceres	09301708	170	0.032	0.026	-0.004	0.005	0.015	0.015
Ceres	111018	170	0.031	0.033	0.022	0.021	0.027	0.005
Neptune	13303002	170	0.024	0.023	0.029	0.028	0.026	0.004
Vesta	24401514	170	0.025	0.040	0.042	0.025	0.033	0.008
Ceres	27505411	170	0.040	0.044	0.011	0.016	0.028	0.014
Neptune	33503508	170	0.039	0.027	0.043	0.040	0.037	0.006
Ceres	57902212	170	0.085	0.049	0.091	0.061	0.072	0.017
Ceres	09301405	180	0.072	0.054	-0.003	0.011	0.033	0.031
Neptune	13303302	180	0.027	0.030	0.039	0.030	0.032	0.005
Herculina	18202805	180	0.130	0.082	0.077	0.084	0.093	0.022
Vesta	24400605	180	0.037	0.026	0.033	0.031	0.032	0.004
Pallas	25101305	180	0.066	0.051	0.056	0.047	0.055	0.007
Ceres	27504805	180	0.057	0.067	0.023	0.018	0.041	0.021
Uranus	32803108	180	0.036	0.032	0.052	0.034	0.039	0.008
Neptune	35600902	180	0.042	0.038	0.048	0.031	0.040	0.006
Neptune	49602004	180	0.040	0.038	0.051	0.038	0.042	0.006
Ceres	59402304	180	0.031	0.040	0.035	0.027	0.033	0.005
Ceres	09301102	200	0.097	0.066	-0.002	0.017	0.045	0.039
Ceres	111018	200	0.091	0.086	0.055	0.043	0.069	0.020
Neptune	13302401	200	0.052	0.043	0.057	0.048	0.050	0.005
Herculina	18202401	200	0.069	0.074	0.082	0.088	0.078	0.007
Vesta	24400302	200	0.061	0.033	0.046	0.050	0.047	0.010
Vesta	24400605	200	0.098	0.063	0.030	0.047	0.059	0.025
Pallas	25101002	200	0.061	0.047	0.059	0.057	0.056	0.005
Ceres	27504502	200	0.093	0.063	0.028	0.033	0.054	0.026
Neptune	32801702	200	0.057	0.043	0.057	0.051	0.052	0.006
Uranus	32802502	200	0.047	0.036	0.043	0.047	0.043	0.005
Neptune	49601802	200	0.053	0.046	0.058	0.050	0.052	0.004
Uranus	55204704	200	0.051	0.054	0.054	0.050	0.052	0.003
Ceres	57901304	200	0.107	0.077	0.047	0.059	0.072	0.023

Table 12: The target list and the individual measurements for the derivation of $f_{psf}(92\sqrt{2})$.

target	TDT	wavelength	pix 1	pix 2	pix 3	pix 4	mean	rms
Ceres	09302314	120	0.049	0.043	0.054	0.039	0.046	0.006
HR5340	07707505	120	0.057	0.050	0.089	0.073	0.067	0.015
Neptune	13302502	120	0.040	0.033	0.062	0.046	0.045	0.011
Herculina	18203108	120	0.091	0.059	0.092	0.082	0.081	0.013
Vesta	24400908	120	0.053	0.055	0.083	0.052	0.061	0.013
Pallas	25101608	120	0.085	0.062	0.100	0.075	0.080	0.014
HR5340	27503008	120	0.061	0.055	0.087	0.064	0.067	0.012
Ceres	27505108	120	0.076	0.060	0.082	0.061	0.070	0.010
Uranus	32802805	120	0.060	0.040	0.071	0.049	0.055	0.011
Neptune	33502902	120	0.060	0.045	0.078	0.056	0.060	0.012
Uranus	55204908	120	0.058	0.055	0.071	0.049	0.058	0.008
Ceres	57901808	120	0.072	0.058	0.093	0.061	0.071	0.014
Ceres	09302011	150	0.071	0.065	0.039	0.034	0.052	0.016
HR5340	07708111	150	0.059	0.051	0.110	0.076	0.074	0.023
Ceres	111018	150	0.050	0.064	0.069	0.045	0.057	0.009
Neptune	15400602	150	0.072	0.053	0.081	0.063	0.067	0.010
Herculina	18203411	150	0.136	0.095	0.110	0.117	0.114	0.015
Vesta	24401211	150	0.081	0.088	0.100	0.077	0.086	0.008
Pallas	25101911	150	0.116	0.101	0.132	0.115	0.116	0.011
HR5340	27503311	150	0.089	0.064	0.095	0.093	0.085	0.012
Ceres	27505411	150	0.083	0.086	0.078	0.076	0.081	0.004
Uranus	32803411	150	0.064	0.055	0.068	0.061	0.062	0.005
Neptune	33503205	150	0.085	0.067	0.102	0.081	0.084	0.012
Ceres	59402708	150	0.096	0.063	0.119	0.086	0.091	0.020
Ceres	09301708	170	0.058	0.059	0.040	0.031	0.047	0.012
Ceres	111018	170	0.057	0.061	0.064	0.051	0.058	0.005
Neptune	13303002	170	0.069	0.050	0.068	0.066	0.063	0.008
Vesta	24401514	170	0.077	0.094	0.111	0.078	0.090	0.014
Ceres	27505411	170	0.078	0.077	0.067	0.055	0.069	0.009
Neptune	33503508	170	0.103	0.067	0.099	0.086	0.089	0.014
Ceres	57902212	170	0.129	0.100	0.139	0.108	0.119	0.015
Ceres	09301405	180	0.111	0.097	0.052	0.047	0.077	0.028
Neptune	13303302	180	0.076	0.057	0.078	0.066	0.069	0.008
Herculina	18202805	180	0.203	0.129	0.126	0.150	0.152	0.031
Vesta	24400605	180	0.105	0.068	0.082	0.076	0.083	0.014
Pallas	25101305	180	0.132	0.103	0.118	0.111	0.116	0.011
Ceres	27504805	180	0.106	0.108	0.074	0.074	0.090	0.016
Uranus	32803108	180	0.108	0.071	0.110	0.074	0.091	0.018
Neptune	35600902	180	0.122	0.083	0.105	0.078	0.097	0.018
Neptune	49602004	180	0.117	0.090	0.103	0.084	0.098	0.013
Ceres	59402304	180	0.124	0.113	0.115	0.098	0.112	0.009
Ceres	09301102	200	0.130	0.111	0.056	0.054	0.088	0.033
Ceres	111018	200	0.108	0.108	0.105	0.078	0.100	0.013
Neptune	13302401	200	0.092	0.063	0.101	0.086	0.086	0.014
Herculina	18202401	200	0.134	0.105	0.132	0.167	0.135	0.022
Vesta	24400302	200	0.104	0.064	0.088	0.103	0.090	0.016
Vesta	24400605	200	0.143	0.090	0.092	0.108	0.108	0.021
Pallas	25101002	200	0.119	0.082	0.121	0.117	0.110	0.016
Ceres	27504502	200	0.164	0.104	0.082	0.097	0.112	0.031
Neptune	32801702	200	0.123	0.080	0.107	0.099	0.102	0.015
Uranus	32802502	200	0.107	0.063	0.095	0.091	0.089	0.016
Neptune	49601802	200	0.108	0.077	0.107	0.099	0.098	0.013
Uranus	55204704	200	0.100	0.080	0.076	0.097	0.088	0.010
Ceres	57901304	200	0.148	0.114	0.112	0.108	0.120	0.016

Table 13: The target list and the individual measurements for the derivation of $f_{psf}(92)$.